Bone, Volume 155, February 2022, Article number 116265
DOI: 10.1016/j.bone.2021.116265

Assessing bone maturity: compositional and mechanical properties of rib cortical bone at different ages

Andrea Bonicelli[1,2], Elena F. Kranioti[3], Bledar Xhemali[4], Emily Arnold[2], Peter Zioupos[2*]

[1] *Faculty of Health and Life Sciences, Northumbria University, Newcastle Upon Tyne, UK*

[2] *Musculoskeletal & Medicolegal Research Group, Cranfield University, Defence Academy of the UK, Shrivenham, UK*

[3] *Department of Forensic Sciences, Faculty of Medicine, University of Crete, Heraklion, Crete, Greece.*

[4] *Institute of Forensic Medicine, Tirana, Albania*

Abstract

Understanding what maturity entails for bone, when it arrives, and its pre- and post-maturity traits and properties is very important for understanding its evolution and physiology. There is a clear but fine distinction between the chronological age of bone (the age of its donor) and the tissue age of the bone packets it comprises at the microscopic level. Whole bone fragility changes with age due to mass and architecture effects, but so do the properties of bone at the tissue level. Tissue age and tissue-level properties are therefore increasingly attracting a great deal of attention recently. The present study investigated compositional and material changes in the hydroxyapatite crystals, the collagenous phase, changes in bone matrix composition and its nanoindentation properties and their decline with chronological age in later life. The aim was to track the age threshold at which cortical bone arrives at maturity and what happens following that threshold. To do so FTIR, DSC/TGA, XRD, nanoindentation and microindentation were used to investigate rib cortical bone material across a cohort of 86 individuals from one ethnic group with age spanning between 17 and 82 years. Results of this cross-sectional study showed a clear increase in mineral content relative to the organic and water contents across all ages. Furthermore, an increase in crystal size and consequent decrease in strain (coherence length) was detected associated with secondary mineralisation and an increase in carbonate substitution. Overall, we observe a number of modifications which contribute to a typical functional behaviour of bone showing an increase in both indentation modulus and hardness until the age of about 35 after which both of these properties decline gradually and concomitantly to other physicochemical changes and seemingly until the end of one's life.

Keywords: maturity; bone properties; tissue age; physicochemical characterisation; nanoindentation.

***Corresponding author:** p.zioupos@cranfield.ac.uk; Musculoskeletal & Medicolegal Research Group, Cranfield University, Shrivenham, SN6 8LA, UK; tel. +44 7754772803

1 Introduction

The very tissue substance of bone changes throughout life from birth to death and somewhere in between goes past the point where it reaches maturity. Generally speaking, bone is a three-phase composite material comprising organic (most of which is a strong load bearing structural protein collagen type-I bathed in non-collagenous proteins), mineral (non-stoichiometric hydroxyapatite (HAp) and water. The organic phase offers a template for embedded HAp crystals lying along their 'c' crystallographic which also aligns along the main axis of collagen fibrils. [1,2]. At the molecular level, collagen is made of three chains of about 1000 amino acids containing the periodically repeating - (Gly-X-Y) n - triplet unit, with X and Y being proline and hydroxyproline residues and Gly is glycine. Of the three chains two of them are α1 and one α2 organised in a triple helix structure: this molecule is called procollagen. Stability of this configuration is given by the hydrogen bonds created between the hydroxyl groups of Y and H_2O. Calcium hydroxyapatite (HAp) the mineral constituent of bone is poorly crystalline containing PO_4^{3-}, Ca^{2+} and OH^- according to the general unit formula $Ca_5^{2+}(PO_4^{3-})_3(OH^-)_2$, with also the presence of CO_3^{2-}. In terms of size and geometry, bone crystals have an elongated shape along their 'c'axis, approximately 30-50 nm long, 15-40 nm wide and 2-10 nm thick with measurements, however, varying with location and the type of bone [1]. The physics and chemistry of bone and its composition are adapted to resist fracture by maintaining an optimal balance between stiffness (resistance to deformation), strength (maximum stress to failure) and toughness (ability to absorb energy) [3]. The increase in bone fragility with age has been largely attributed to the decrease in bone mass and alterations in the micro-

architecture of both cortical (e.g., increase in porosity, cortical thinning) and trabecular bone (increase in trabecular spacing and decrease in thickness and number of trabeculae) [4,5]. Beyond these macroscopically observed changes, there are other changes in composition and the mineralisation profile of bone matrix, which are also very important, but which are more subtle. Bone mineralisation process, for instance, passes from a phase of modelling before maturity to mostly remodelling post-maturity. It is also highly dependent on the rate of remodelling whereby slow remodelling would allow more time for secondary mineralisation resulting in tissue containing longer and more crystalline HAp crystals. By contrast, in modelling when bone turnover is fast (e.g., in young individuals) crystals have less time to mature and the matrix itself is less mineralised. The mineral maturation process involves ion substitution and entails an increase in both crystal size and crystallinity [6,7]. Similarly, a number of post translational modifications of collagen fibres have been seen to affect bone mechanical properties [4,5,8,9]. There is a reduction of approximately 40% in the number of hydroxypyridinium crosslinks linked to β-amino-proprionitrile. Collagen changes affect stiffness, strength, and post-yield deformation of bone at the macroscopic level by approximately 60% [8,9] and it has been reported in literature that degeneration of the organic matrix with age is responsible for the increase of risk of fracture [4,5,10]. At bone tissue level the effect of the increase in mineralisation with age is not always easy to interpret. Bala et al. [6,11] suggested this phenomenon correlates with an increase in hardness and elastic modulus in both cortical and trabecular bone. The result of maturation of the collagen moiety of bone manifests in changes in ability of bone to deform plastically and sustain damage resulting in reduced toughness [5,8,9]. Overall, ageing appears to affect the content and the quality of both the mineral and collagen phases, in turn affecting the properties of the bone matrix (the tissue that bones are made of) which results in bone itself becoming more brittle [9,12]. Although we have a good understanding of some of the processes which underpin the maturation of bone matrix and the implications of this maturation for bone fragility, we need to understand when these processes happen and to record when the biological body switch turns from ‘on’ to ‘off’, from modelling to the remodelling phases of bone. The present study uses a range of physicochemical tests to track down the processes that happen at the bone tissue level in samples ranging from 17 to 82 years of age and so pinpoint the age at which bone tissue passes from pre- to post- maturity.

2 Material and methods

2.1 Study sample and preparation

The autopsy material was received from the Institute of Forensic Medicine in Tirana in dry ice and was kept at -20°C and kept in physiological buffered solution fully hydrated between preparation and experimental procedures. The collection was composed of small sections taken from the sternal end of the fourth right rib of 85 individuals (Full details in Table-S1 in the supplementary material section-1) ageing 17 to 82 years (mean age 45.61 ± 19.98 SD), 58 males (mean age 44.78 ± 17.46) and 27 females (mean age 47.41 ± 17.29 SD). For nanoindentation three mm thick sections were cut by using a Struers Accutom wafering saw equipped with 300 µm wide diamond impregnated blade irrigated using deionised water. Sections were cleaned following a protocol involving spinning in plastic falcon tubes in a 1:1 Chloroform-Methanol mixture for 36 h. The solution was flushed by gradually returning to 100% ethanol for 12 h and then was gradually fully rehydrated at grades of 70%, 50% 30% over 24 hrs, and returned to physiological solution for storing. After drying for 24 h at room temperature, the sections were embedded in resin (Metprep Kleer Set Type SSS). The resin simply holds the sample firm for preparation and testing and does not penetrate the bone porosity (no vacuum extraction is used), it sets quickly, and it is cold curing to avoid tissue damage. Samples were then metallographically polished using an automatic Struers RotoPol-15 with 203 mm silicon carbide abrasive disks grinding paper of decreasing grit size (400, 800, 1200, 2500) and finished MasterTex cloth with Alumina 3B 6oz 0.05 µm. The rest of the bone sample was shared between the different physicochemical tests. Bone marrow was removed by warm water pressure jet and a scalpel was used to scrape off the trabecular bone retaining the cortical bone. This material too was degreased by the previous method and was processed into powder using a Retsch Mixer mill 2000 by cycling for 1 min and at 60 Hz. In between the two different cycles the powder was filtered using a 106 µm sieve to produce a more uniform size mixture and eliminate larger particles that could affect heat absorption and X-ray diffraction [13]. Full details of these preparation protocols and methods are also contained in two recent studies [14, 15] produced to predict the ‘age-at death’ of individuals for use with recovered skeletal remains in the forensic context.

2.2 Nanoindentation, microindentation and porosity assessment

A CSM-NHT (system v.3.75, CSM, 2034 Peseux, Switzerland) instrument was used to perform nanoindentation testing. The instrument was operated at 10 mN maximum hold load (20 mN/min loading/unloading speed) with 30s long load/hold/unload stages. A total 10 indentations were performed for four different secondary osteons. This procedure was repeated for four areas located two on the pleural surface (concave facing the thoracic

cavity) and two on the cutaneous surface (convex facing the skin). Universal Hardness (H) was calculated from load and contact area (**Eq. 1**), The nanoindentation modulus (E_{IT}) was obtained in the unloading phase as per the Oliver and Pharr method (**Eq. 2**).

$$H = \frac{P_{max}}{A} \quad (1)$$

$$E_r = \{ \pi^{½}/2\beta \} \ \{S / A^{½}\} \quad (2a)$$

$$E^* = \{ E_{IT} / (1-\nu_s^2)\} = \{ 1/ E_r - (1-\nu_i^2) / E_i \}^{-1} \quad (2b)$$

where the reduced modulus E_r is produced from the stiffness S in the retracting phase, the contact area function A and the shape factor β. The plain strain modulus E^* derives the nanoindentation modulus E_{IT} for a sample Poisson's ratio value of $\nu_s = 0.3$, with elastic properties of the diamond indenter $\nu_i = 0.07$ and $E_i = 1140$ GPa. Fused silica (with a known value of modulus of 72 GPa, ν_s =0.17) was used to calibrate the tip shape function and gave E_{IT} values of 72.14 ± 2.5 GPa (mean± standard deviation, N=14 at 10 and 20mN) in a pre-test calibration check. Indentation creep (C_{IT}) was calculated by the proportional increase in depth (**Eq. 3**) occurring while the load is constant at max load (for 30s) and it reflects the viscoplasticity of the tissue. The elastic work ratio (η_{IT}) was obtained by examining the percentage ratio of the elastically recovered energy over the total energy (elastic + plastic) input during performing an indentation sequence (**Eq. 4**, where W represent the area under the curve). Values for both areas were averaged in order to obtain mean tissues values to be compared with matrix physicochemical parameters.

$$C_{IT} = \frac{h_1 - h_2}{h_1} \times 100 \quad (3)$$

$$\eta_{IT} = \frac{W_{elast}}{W_{elast}+W_{plast}} \times 100 \quad (4)$$

During the test, attention was paid in avoiding factors that produce 'experimental noise', such as levelling the sample to allow the indenter to penetrate at right angles, minimising the external vibrations and discarding any asymmetric or problematic readings. Ten locations per each osteon and its adjacent interstitial area (**Fig. 1**) were tested in order to obtain a meaningful mean value and avoid any effects to do with the radial distance from the central lumen of the osteon or the interlamellar differences [16].

Figure 1

An INDENTEC HWDM-7 instrument, equipped with a square-shaped pyramid diamond tip of $\theta = 136°$, was employed to produce Vickers microhardness (HV) values for osteonal and interstitial bone areas for each specimen. The maximum load in these tests was set at 10 gf. The same areas selected for nanohardness testing were examined applying one indentation on the osteon and one on the surrounding matrix for a total of 4 couples of indentations per section, one per quadrant.

Optical porosity ($PoAr_{\%}$) was obtained from these transverse sections by taking four images for each specimen with a reflected light microscope at ×20 and the use of ImageJ. Four locations were selected in order to sample the entire cortical area in the four quadrants, two sites on the pleural surface and two from the cutaneous surface. Each picture was cropped to select areas completely occupied by bone and converted into 16-bit images (Image > Type > 16-bit). The plugin BoneJ was employed to automatically calculate area fraction by applying a threshold mask (Plugins > BoneJ > Volume Fraction) [14,15].

2.3 Thermal analysis

Thermogravimetric analysis and Differential Scanning Calorimetry were performed using a TGA/DSC3+ (Mettler Toledo, Indium calibrated). A first increase in temperature between 25°C and 550°C at 10°C/min was followed by an isothermal combustion over 10 min at 550°C to completely remove the organic components and obtain ash content. Temperature in the chamber was controlled by a continuous flow of water at room temperature. The bone material was tested in air in 20 µL aluminium pans with flat bases filled with ~10 mg of bone powder for which the weight was recorded using a microbalance (Sartorius Genius ME235), while an empty crucible was used as a reference. With this instrument thermogravimetric and calorimetry analysis were carried out simultaneously and on the same sample and this enhances the consistency of the produced data. The entire analysis was carried out using StarE V 15.0 software after normalizing the results to sample size. Quantitative investigation involved the calculation of the percentage value of the two major weight losses in the TGA curve by linear tangent [14–15] between temperature thresholds: ~50-120°C and ~200-550°C. Ash

weight was calculated in an Excel spreadsheet by subtracting water and organic percentage weight loss values from 100. The same temperature intervals were taken as references in order to analyse linear integration values for enthalpy variation. The powdered samples started from room temperature to 550°C. The question is then if the water measured up to 200°C is surface or bound water [17]. Unal and Akkus [18] suggested that a negative correlation between water content and porosity is indicative of structurally bound water, while the opposite behaviour would suggest the presence of surface water. Here we obtain a negative correlation between these two parameters (R = -0.27, p = 0.012) which indicates that we have recorded structurally bound water.

2.4 Fourier transform infrared spectroscopy (FTIR)

For spectroscopic analysis, data were collected by means of ALPHA T Platinum spectrometer (Bruker Optics) in attenuated total reflectance mode (ATR). The range of interest was 4000-400 cm^{-1} with 4 cm^{-1} resolution for a total of 64 scans. Approximately 3 mg (∼106 μm particle size) of bone powder were analysed cleaning the holder and the crystal with deionised water after each measurement. The measurements for the entire sample were carried out in the same conditions to maximise consistency. Spectral analysis was performed in Spectrum software 10.2 (Perkin Elmer). Due to the high variation in the spectra profiles due to levels of hydration of the powder, contact area between the crystal and the sample and amount of powder used during the examination spectra were not directly comparable. The aim of this examination is to offer semi-quantitative information on the mineral to organic and the carbonate to phosphate ratio of the bone matrix. Mineral to organic matrix ratio (MM) was calculated by the integrated area under the $v3PO_4^{3-}$ bands (1200–900 cm^{-1}) and amide I (1750–1600 cm^{-1}) [19] and represents the amount of collagen normalized to the amount of mineral. Similarly, carbon substitution [19] (carbonate to phosphate ratio) was calculated by the band $v2CO_3^{2-}$ (890–850 cm^{-1}) over $v3PO_4^{3-}$ (1200-900 cm^{-1}). Finally, mineral crystallinity was calculated according to Thompson et al. [20] investigating the distance between symmetric bands 565 cm^{-1} and 605 cm^{-1} of $v4PO_4^{3-}$. Parameters and calculations are reported in **Table 1**.

Table 1 FTIR parameters (A: absorbance; I: intensity).

Parameter	Calculation	Explanation
MM	$A_{1200-900}$ / $A_{1750-1600}$	Integrated value of $v3PO_4^{3-}$ over Amide I bands
CP	$A_{890-885}$ / $A_{1200-900}$	Integrated value of band $v2CO_3^{2-}$ over $v3PO_4^{3-}$ bands
CI	$I_{605} + I_{565}$ / I_{595}	Mineral crystallinity index calculated by the intensity of the $v4PO_4^{3-}$

2.5 X-ray diffraction (XRD)

A pXRD sample holder with a glass spacer was filled with bone powder for XRD analysis. PANalytical X'Pert PRO Multi-Purpose Diffractometer by means of a Cu K_α radiation was employed for the characterisation. Data collection was carried out across an angular range of 15–80 2θ (°) (5.90–1.20 Å) using a PIXcel strip detector at a count rate of ∼1 s. Data was also collected for two further stepped scans under the same sample conditions but across an angular range of 23–27 2θ (°) (3.86–3.30 Å d-spacing) and 50–55 2θ (°) (1.82–1.67 Å d-spacing), and with a count time at each step equivalent to ∼3 s. The two additional stepped scans were collected to provide greater quality data at the 002 and 004 Bragg maxima respectively, from these data the full width at half maximum (FWHM) of the peaks 002, 004 (crystal length along the c-axis), 210 (reflection perpendicular to the 'c'axis) and 030 (representing basal plane on its smallest dimension, interpreted as crystal thickness). Bruker Topas software (Version 4.1, 2008) was employed to undertake profile fitting of each diffraction profile. This provided quantitative crystallite size and morphology parameters through calculation of the coherence length and structural parameters of the crystal lattice through the lattice parameters. Coherence length was calculated for the orthogonal crystallographic direction ⟨00ℓ⟩, ⟨hk0⟩ and ⟨0k0⟩ using the Scherrer equation (**Eq. 5**), which uses the instrument corrected, full width at half maximum of the desired peak. The lattice parameters were calculated from whole pattern fitting refinement of diffraction profiles to obtain the 2θ peak positions.

$$CL = \frac{K\lambda}{\beta \cos\theta} \quad (5)$$

Where K is the Scherrer constant (0.9), λ is the wavelength and θ the Bragg angle.

Coherence length is the measurement of mean distance within a crystal that lattice order persists. Increase in coherence length is the result of decrease in the magnitude of peak broadening therefore can be used as a quantitative measure of crystallinity. It can be suggested that it is directly proportional to crystallite size (physical dimension of crystals) and inversely to strain (crystal imperfection).

However, profile fitting along ⟨hk0⟩ and ⟨0k0⟩ crystallographic directions are unreliable due to peak overlapping and therefore accurate separation of crystallite size and strain for the associated directions does not provide sufficient reliability. As a result, coherence length in the ⟨00ℓ⟩ direction from the 002 and 004 maxima were used to calculate crystallite size and non-uniform strain by means of the Williamson-Hall (W-H) [21,22]. The method allows to overcome the issue of anisotropy of mineral crystals according by segregated into crystallite size and non-uniform strain. W-H plot was calculated according to **Eq. 6**, where L is crystallite size and ε non-uniform strain.

$$\beta cos\,\theta = 4\varepsilon\, sin\,\theta + \frac{k\lambda}{L} \quad (6)$$

2.6 Statistical analysis

Statistical analysis was carried out in R 3.6.0. Normality was evaluated by Saphiro-Wilk test (at p = 0.05), skewness and kurtosis. Paired t-tests (for each donor osteon vs interstitial) were used to compare differences. Statistical tests were considered significant at p = 0.05. Following an initial analysis which showed the age threshold for maturity was at 35 years we produced Pearson's correlations for the sample split in two for < 35 and > 35 years to quantitatively evaluate maturity for the different parameters. Table 2 lists all parameters and their units for all experimental methods.

Table 2 Full set of parameters with abbreviation, instrument, units, and descriptive statistics (SD: standard deviation).

Parameter	Abbreviation	Instrument	Unit	Mean	SD
Optical porosity	Po.Ar%	BoneJ	%	5.75	1.91
Nanoindentation/ nanohardness (in Vickers equivalent units)	H	Nanoindentation	kgf/mm^2	46.37	9.18
Nanoindentation modulus	E_{IT}	Nanoindentation	GPa	18.90	2.34
Nanoindentation creep	C_{IT}	Nanoindentation	%	4.96	0.66
Nanoindentation elastic work ratio	η_{IT}	Nanoindentation	%	21.42	1.92
Microhardness (Vickers units)	HV	Microindentation	kgf/mm^2	41.32	5.46
Collagen thermal degradation enthalpy change	LΔH	TGA/DSC3+	Wg^{-1}	160.78	160.78
Organic combustion enthalpy change	CΔH	TGA/DSC3+	Wg^{-1}	3251.68	243.09
Bound water	W	TGA/DSC3+	wt%	8.74	0.60
Organic phase	Or	TGA/DSC3+	wt%	28.03	1.02
Mineral content	Ash	TGA/DSC3+	wt%	63.23	1.36
Mineral/Organic ratio	MM	ATR-FTIR	ratio	6.98	0.55
Carbonate/phosphate ratio	CP	ATR-FTIR	ratio	0.018	0.002
Crystallinity	CI	ATR-FTIR	ratio	1.007	0.035
Mineral strain	Strain	XRD	%	0.671	0.135
Mineral Size	Size	XRD	nm	32.26	2.59
Coherence length at 002 peak	CL002	XRD	nm	23.85	0.86

Coherence length at 004 peak	CL004	XRD	nm	18.99	1.02
Coherence length at 210 peak	CL210	XRD	nm	9.66	0.95
Coherence length at 030 peak	CL030	XRD	nm	8.26	0.44
Lattice parameter	'a'axis	XRD	Å	9.416	0.003
Lattice parameter	'c'axis	XRD	Å	6.903	0.003

3 Results

3.1 Across the entire age range

Nanoindentation and microindentation was applied in total in 344 osteons and the surrounding interstitial matrix areas. Pairwise t-test statistics (Table 3) demonstrated significant difference between these two areas for all the variables. For nanohardness (H_{IT}) and microhardness (HV), indentation modulus (E_{IT}) and creep (C_{IT}) values are higher for interstitial bone compared to osteons while elastic work ratio (η_{IT}) shows higher values for osteons. With respect to age there was no significant relationship for H_{IT}, HV and E_{IT}, but there was a negative correlation for C_{IT} (R = -0.37) and a positive one for η_{IT} (R = 0.48) when looking across the entire age range ($p < 0.01$).

Table 3 Results for pairwise t-test comparison between the average indentation values for each donor in osteons and interstitial bone and across all ages (SD = standard deviation, CI = confidence interval for the difference).

Variable	Osteon		Interstitial		Paired t-tests	
	Value	SD	Value	SD	95% CI	p-value
H_{IT}	44.03	8.89	48.83	10.04	[-5.872, -3.724]	<0.001
E_{IT}	17.52	2.19	20.31	2.68	[-3.120, -2.474]	<0.001
C_{IT}	4.75	0.73	5.18	0.64	[-0.531, -0.341]	<0.001
η_{IT}	21.87	2.11	20.96	1.87	[+0.660, +1.156]	<0.001
HV	33.85	5.30	39.65	5.17	[-6.561, -5.036]	<0.001

Further correlations across the entire age range are shown in **Table 4** as well as the correlations between the structural and micromechanical parameters. Optical porosity, collagen thermal stability and enthalpy values, as well as ash weight and organic content correlate significantly and positively with age. There was a significant positive correlation in carbonate to phosphate ratio (R = 0.50) throughout life accompanied by a moderate negative trend in crystallinity index calculated from $v4PO_4^{3-}$. Changes in crystal geometry was further evaluated by means of powder XRD. We found, by means of W-H plot, non-uniform strain increasing significantly with age as well as a weak positive relationship in size. This is also combined with a mild negative change in CL004 suggesting a positive significant trend in the crystal size along the main axis of the crystal combined with the negative in lattice disorder. Finally, CL030 shows a minor, though significant, positive correlation with age. Overall, we found positive correlation with mineral content at the expense of organic content combined with a negative correlation for carbonate to phosphate ratio and crystal size.

Table 4 Correlation coefficient values for indentation mechanical properties, age, and physicochemical changes of the entire age range sample ($p < .0001$ '****'; $p < .001$ '***', $p < .01$ '**', $p < .05$ '*').

Full Sample	Age	H_{IT}	E_{IT}	C_{IT}	η_{IT}	HV
Age	1	-0.1	-0.17	-0.37***	0.48****	0.13
Po.Ar%	0.87****	-0.04	-0.13	-0.33**	0.38***	0.11
LΔH	-0.35**	0.05	0.06	0.24*	-0.26*	-0.08

CΔH	-0.26*	-0.08	-0.09	0.25*	-0.21*	-0.26*
W	-0.24*	-0.24*	-0.23*	0.26*	-0.29**	-0.36***
Or	-0.37***	-0.27*	-0.28**	0.38***	-0.39***	-0.51****
Ash	0.38***	0.31**	0.31**	-0.40***	0.42****	0.54****
CP	0.50****	-0.33**	-0.32**	-0.17	0.27*	-0.14
CI	-0.27*	0.37***	0.37***	0.02	-0.15	0.28*
MM	0.08	0.26*	0.28**	-0.23*	0.27*	0.40***
Strain	0.27*	-0.53****	-0.47****	0.04	0.12	-0.34**
Size	0.22*	-0.09	-0.06	-0.11	0.2	0.03
CL002	-0.05	0.61****	0.58****	-0.21	0.11	0.53****
CL004	-0.23*	0.70****	0.65****	-0.14	-0.03	0.50****
CL030	0.22*	-0.02	-0.29**	0.23*	0.11	-0.01
CL210	0.07	0.20	0.00	0.10	0.25*	0.16
‘a’axis	-0.22*	0.22*	0.19	-0.08	-0.02	0.15
‘c’axis	-0.11	0.19	0.16	0.02	-0.13	0.07

The nanoindentation parameters (E_{IT}, H_{IT}, C_{IT}, η_{IT}, values averaged for each donor) correlated with mineral, water, and organic contents across the whole age range; there was a negative trend with the carbonate to phosphate ratio, positive significant correlations were present between E_{IT}, H_{IT} and mineral content and crystallinity. E_{IT}, H_{IT} had strong positive relation to crystallite size along the ⟨00ℓ⟩ crystallographic direction (CL002 and CL004) indicating that both mineral content as well as crystal growth relate to elastic modulus and hardness at the bone tissue level. Indentation creep (C_{IT}) and the elastic work ratio (η_{IT}), which are both indicative of viscoplasticity and brittleness of the material, were by and large related to the mineral and organic content, the age and the porosity but were generally unaffected by the qualitative aspects of the mineral crystal chemistry (by that we mean practically all of the ten parameters produced by FTIR-ATR and XRD).

3.2 Is there a maturity threshold?

It is the main objective of this work to define bone properties with respect to its maturity level. For doing so we need to (i) detect any likely maturity threshold and following that clarify ageing structural alterations and (ii) establish cause/effect and structure/function relationships either side of the threshold.

Early inspection of the mechanical, structural, and physicochemical data revealed that there was an inflection point at an age of ~35 years (in the range of 34-37 yrs of age). **Figure 2** shows one such example, the trend of organic content with age (three examples given in Supplementary material section-2), where exploring non-linearity by CR plot (component+residuals in R) and paying attention to the second derivative of the curve shows that there is noticeable change in behaviour from 35 years onwards. Consequently, we have divided the sample for donors below and above 35 years of age and present the data colour coded in these two domains.

Figure 2

Figure 3 shows the evolution of nano/micro-mechanical bone tissue data (average of all indents for each donor) with age. There were highly significant positive relationships ($p < 0.001$) for H_{IT} ($R = 0.51$), E_{IT} ($R = 0.43$) and HV ($R = 0.61$), that is the stiffness and the hardness of the immature portion of the sample (< 35 years). In this same section C_{IT} and η_{IT} were also significantly relating to age negative and positively respectively. After maturity was reached (> 35 years) four out of five parameters were still significantly relating to age although some trends either reversed (E_{IT}, H_{IT}, and HV) or stayed the same (C_{IT} and η_{IT}). In all ten trends (2 trends x 5 parameters before and after 35 years) only one (C_{IT} after 35 years) was insignificant with age. Worth reporting here that there was one noticeable qualitative difference between these nanomechanical parameters: while

stiffness and hardness (E_{IT}, H_{IT} and HV) reversed their trends before and after maturity, the viscoplasticity and energy ones (C_{IT} and η_{IT}) had the same trend before and after but simply the rate of change with age changed pre- and post-maturity (**Fig. 3**).

Figure 3

3.3 Composition and physicochemical characterisation of bone matrix for maturity assessment

We examined subsequently the evolution of the rest of the physicochemical properties pre- and post-maturity. There were three specific patterns for trends with age in which the bone composition could be divided: (i) variables that showed an inflection at 35 years of age (similar to that seen for tissue mechanical properties); (ii) variables with a monotonic and statistically significant change with age; (iii) variables that did not show significant relationship to age.

3.3.1 Inflection point at maturity

Figure 4 shows the data from the thermo-gravimetric analysis (TGA) which refers to bone composition throughout age. A two-phase behaviour is evident again with significant positive trend in mineral content (with a concomitant decrease in water and organic contents) up to the age of ~35 years, after which there was no significant change with age. This does not mean of course that bone after 35 enters a state of quiescence, as we know bone is as active as ever and it employs remodelling, damage repair and damage limitation strategies to stay structurally safe. The tissue mechanical changes observed after 35 years may be due to other physicochemical changes and modifications.

Figure 4

From Ash (DSC/TGA) and mineral to matrix ratio (FTIR) mineralisation shows an increment before maturity followed by a moderate negative trend afterwards and coherence length calculated from 004 peak (XRD) shows a tendency to be positively correlated until maturity to then negatively ($P < 0.01$) suggesting a decrease in crystallite length.

3.3.2 Monotonic relationship with age

Intracortical porosity increases monotonically throughout life ($p<0.05$) from a value of 0.03 (3% of the cortical cross-sectional area) to a value of 0.09 (9%) at the ages of 80-85 years. The only two other physicochemical parameters that showed a monotonic behaviour with age are carbonate to phosphate ratio (CP) and crystallinity (CI). Both show the same trend for both age <35 and >35 and with the > 35 years portion been significant at $p < 0.05$. CP shows a constant increase, while CI shows a negative correlation with age. (**Fig. 5**).

Figure 5

3.3.3 No age-related trends

A number of parameters did not show any significant variation with age overall, or in the two age periods. The DSC rate of enthalpy values for collagen thermal degeneration showed a small insignificant decline with age. This was also the case for CL calculated at ⟨hk0⟩ and ⟨0k0⟩ directions, which provides an indication of crystal growth in width and thickness (with one exception for CL030 showing a positive trend across the whole age range at $p > 0.05$ (**Fig. 5**). Similarly inconclusive was the analysis of trends of values for lattice parameters.

3.4 Interaction between structure and function

The data produced here provided homogenised bone tissue composition and physicochemical properties and nano-micro mechanical behaviour from the same samples making it possible to look for interrelationship between structure and function for pre- and post-maturity.

3.4.1 Matrix composition: effect of mineral, organic and water phases

Pre-maturity (<35) matrix composition shows correlation (**Table 5**) with indentation parameters ($p < 0.05$) vs mineral content, positive for four of them and negative for C_{IT}. Post-maturity (>35years) only indentation modulus shows a weak positive correlation while the relationship of the other parameters (H_{IT}, HV, C_{IT}, η_{IT}) with mineral content becomes indeterminant. There is a qualitative difference between the relationship of indentation and mineral content with age before and after maturity. Indentation modulus and hardness show a downward trend after 35 but mineral content reduces only slightly and indeed Fig.6 shows that the effect and

relationship between the two in the remodelling phase after 35 is random. Fig.5A has already shown that the data scatter of porosity values vs age is small before 35 (modelling phase) and increases noticeably after 35 (remodelling phase) perhaps reflecting the disorganised non-prescribed nature of remodelling phase changes.

Figure 6

Pre-maturity collagen content influences bone tissue properties also significantly but in the other direction: with a significant negative correlation with H_{IT} (R = -0.61), E_{IT} (R = -0.51), HV (R = -0.80) and η_{IT} (R = -0.78) and positive for indentation creep (R = 0.74). Similarly, to the mineral content, after 35 years of age no significant trends were identified. As can be seen in **Table 5**, these results are also supported by the data from the spectroscopic quantification of collagen content. The water content for the <35 years old, was influential for indentation creep (R = 0.63), elastic work ratio (R = -0.64) and microhardness HV (R = -0.47). Carbonate to phosphate ratio, which was previously seen (Fig.6b) to positively change across ages it was seen to correlate negatively and significantly with H_{IT} (R = -0.43), indentation modulus E_{IT} (R = -0.41), and hardness HV (R = -0.45).

3.4.2 Mineral crystal size and strain

Crystallite size and strain behaved differently before and after maturity. Strain has a positive correlation with age pre-maturity and negative afterwards. Size negatively correlates with age throughout life. These size changes, however, were not statistically significant, only qualitative and an indication of what is happening at the crystal level. Modifications in crystal size (obtained by W-H plot), although present did not relate to the tissue mechanical properties probably due to size distribution heterogeneity and anisotropy of crystal size. Post-maturity, crystal strain intended here as a semi-quantitative description of intra-crystallite imperfections, was positively and highly significantly correlated with hardness H_{IT} (R = 0.60), indentation modulus E_{IT} (R = 0.54) and microhardness HV (R = 0.58).

The age-related changes in crystallite size along the ⟨00ℓ⟩ direction (major axis of the crystal) showed a positive and then negative trend with age, and in both age periods it related highly significantly to the increase and then a decrease of nano- and micro-hardness, indentation modulus and creep. This by no means implies a cause-effect relationship as it mirrors the behaviour of the mineral content with which it goes hand in hand. Both carbonate to phosphate ratio and crystallinity change with age and they cross correlate with tissue mechanical properties, but similarly to crystallite size, they may do so indirectly through composition (the mineral content of bone in both phases).

Lastly, the lattice parameter, along the 'a' and 'c' axes showed positive significant correlation only with nano- and micro-hardness and not with indentation modulus. This contrasting result, the differential relational behaviour to stiffness-vs-hardness may be important in understanding bone plasticity (hardness is related to yield properties) as opposed to bone deformation (stiffness). The correlation coefficients results are shown in **Table 5**.

Table 5 Correlation coefficient values for indentation mechanical properties vs composition and physicochemical changes, with the sample split for pre- and post-maturity ($p < .0001$ '****'; $p < .001$ '***', $p < .01$ '**', $p < .05$ '*').

< 35	**Age**	**H_{IT}**	**E_{IT}**	**C_{IT}**	**η_{IT}**	**HV**
Age	1	0.51**	0.43*	-0.63***	0.54**	0.61***
Po.Ar%	0.75****	0.33	0.18	-0.43*	-0.26	0.30
LΔH	-0.23	0.04	0.09	0.42*	-0.37	-0.08
CΔH	-0.33	-0.09	-0.08	0.38	-0.29	-0.17
W	-0.57**	-0.25	-0.16	0.63***	-0.64***	-0.47*
Or	-0.72****	-0.61***	-0.51**	0.74****	-0.78****	-0.80****
Ash	0.74****	0.54**	0.43*	-0.78****	0.81****	0.76****
CP	0.34	-0.29	-0.29	-0.27	0.19	-0.01
CI	-0.14	0.39*	0.35	-0.02	0.07	0.22
MM	0.28	0.51**	0.52**	-0.35	0.52**	0.68***

Strain	-0.14	-0.45*	-0.37	0.24	-0.08	-0.28
Size	0.07	0.00	0.05	-0.08	0.2	0.03
CL002	0.28	0.62***	0.60**	-0.42*	0.36	0.41*
CL004	0.27	0.66***	0.59**	-0.42*	0.27	0.42*
CL210	0.12	0.32	0.21	-0.51**	0.37	0.27
CL030	0.28	0.13	0.15	-0.05	0.18	0.21
'a'axis	-0.08	0.16	0.22	0.06	-0.16	0.03
'c'axis	-0.002	-0.004	0.0023	0.04	-0.28	-0.15
> 35	**Age**	**H_{IT}**	**E_{IT}**	**C_{IT}**	**η_{IT}**	**HV**
Age	1	-0.44***	-0.51****	-0.18	0.33*	-0.44***
Po.Ar%	0.77****	-0.23	-0.32*	-0.15	0.21	-0.29*
LΔH	-0.05	0.11	0.09	-0.01	0.01	0.14
CΔH	0.02	-0.05	-0.07	0.07	-0.01	-0.17
W	0.11	-0.21	-0.24	-0.02	0.02	-0.18
Or	0.14	-0.06	-0.17	0.03	0.06	-0.16
Ash	-0.17	0.17	0.27*	-0.01	-0.06	0.23
CP	0.47***	-0.43***	-0.41**	0.02	0.16	-0.45***
CI	-0.30*	0.38**	0.39**	-0.01	-0.18	0.40**
MM	-0.31*	0.15	0.19	-0.09	0.05	0.20
Strain	0.25	-0.60****	-0.54****	0.07	0.1	-0.53****
Size	0.03	-0.16	-0.12	-0.01	0.08	-0.11
CL002	-0.35**	0.60****	0.57****	-0.09	-0.05	0.58****
CL004	-0.34**	0.74****	0.69****	-0.1	-0.09	0.66****
CL210	-0.01	-0.15	-0.14	-0.12	0.06	-0.08
CL030	0.043	0.23	0.24	0.08	0.00	0.26
'a'axis	-0.06	0.28*	0.22	-0.22	0.14	0.34**
'c'axis	-0.02	0.31*	0.25	-0.04	-0.003	0.28*

4 Discussion

The main purpose of the present study is to investigate the onset, advance and occurrence of maturity at the bone tissue level. In the growing phase from birth to skeletal maturity bone builds itself up, in the modelling phase it lays down collagen and takes up more and more mineral, and as a result there is generally a perceived increase in stiffness and strength and a concomitant loss of toughness [23–25]. After skeletal maturity is reached, the threshold of which as shown here for ribs is around the 35year old mark, bone aims to achieve homeostasis in structure and function. After the threshold, in the remodelling phase there is an increase in turnover with bone mass ingredients being replaced constantly in a process of continuous repair and a continuous effort to maintain a status quo in condition and properties [25-27]. This maintenance mechanism is triggered and regulated substantially by endocrine factors at systemic level as well as by mechanical loading and the resulting microdamage accumulation at localised level [23-27].

4.1 Mechanical properties, heterogeneity, and age-related changes

Nanoindentation is suitable for investigating mechanical properties at the bone tissue level and with spatial resolution of ~1 μm or better it can target specific bone microstructures such as osteons, trabeculae, interstitial

areas etc. Our data showed difference in properties between osteonal and interstitial areas with the latter having higher values for indentation modulus, hardness and creep and lower for elastic work ratio (η_{IT}). These results agree with a previous study from Rho et al. [28] and reflect the *in situ* maturation of bone matrix with time versus the newly laid down osteonal material [11,29-31]. In bone osteonal there is a reduction in tissue mineral density. In interstitial bone regions which are historical remnants of bone matrix laid down sometime in the past the bone continues in its course of maturing with more mineral added in and with the crystals themselves maturing, enlarging in size, and changing in their crystallinity and perfection [6,32,33]. However, what is also noticeable is that both kinds of tissue types behave the same in nanoindentation going up/down before/after maturity. That does pose a conundrum, if the process of in situ maturation and mineralisation of bone (from osteoid to fully mineralised tissue) holds true and bone saturated with mineral goes asymptotically to a saturation plateau, why then the interstitial packet areas lose mineral content and show a reduction on nanoindentation property values? The answer is not clear and further studies may be warranted on this subject alone.

4.2 Mechanical properties and mineral modifications

In this study we have found a highly significant relationship between the increase in mineral content and both tissue stiffness and hardness. This dependency to the presence and amount of mineral is present throughout the entire age range 17-84 years old and in all areas of bone. It constitutes then a very basic and fundamental bone tissue-level property which demonstrates the primary evolutionary and diagenetic mechanism bone tissue employs to modify its mechanical characteristics at the microscale (the tissue level) adjusting the mineral content [34–37]. However, by tracking the mineral content pre- and post-maturity we have shown that there is first a mineral content increase in the growth phase which post-maturity is followed by a continuous internal transformation where bone content does not change much but the kind of bone mineral that is resident in the mineralised tissue is altered by ion substitutions, increased carbonate to phosphate ratio, changed crystal size and geometry, and in lattice parameters. We suspect that as a consequence of all these changes, there is probably also a change in the mineral to collagen fibre association and bonding and in the milieu of the non-collagenous proteins (NCP) present, which we did not examine here.

Others have reported similar findings such as that mineral content changes (measured by FTIRM) occur mostly in the juvenile phase of bone development [36] or that the carbonate to phosphate ratio, which is also believed to increase strain in the crystal lattice also induces irregularity in the atomic structure and modifications in crystal geometry [35]. Carbonate to phosphate ratio in the present study showed an increase throughout the entire life span and in later life it had a negative correlation to nanoindentation similar to a previous animal study [38] which suggested that lattice asymmetry introduced by this nonstoichiometric substitution is responsible for the deterioration of mechanical behaviour of cortical bone matrix. Unfortunately, we did not see any clear correlations between age and crystallite strain to confirm this hypothesis with confidence. However, the data overall supports the notion that lattice strain causes vacancies which allow increased ion substitution and resulting in a reduction in crystallinity. This has been shown by others [33,39] where a reduction in bone strength associated with mineral deficiency was also related to a lower degree of crystallinity and higher ion substitution. In the present study crystallinity showed a weak negative correlation with age ($R = -0.27$), but we found a positive relationship between crystallinity and both indentation modulus and hardness, suggesting that crystal size and crystal lattice perfection as well as the integrity of bone matrix may be key to the overall health of bone tissue. After maturity, therefore, crystallinity decreases as remodelling reduces the amount of bone undergoing secondary mineralisation and complete crystal growth.

Regarding crystal size a previous XRD study on iliac spine samples suggests that it increases towards maturity and does not vary afterwards [40]. In contrast, we have found that crystal size along the ‘c’axis (aligned with collagen fibrils) decreases after maturity probably as a result of the increased turnover in the remodelling phase. Although longer crystals may result in stiffer and harder bone matrix this may or may not become apparent at the homogenised level (our tests used bone powder and thus they homogenised/averaged properties) depending on the amount and extent of the remodelling, which produces a mosaic of bone tissue material packets. The coherence length calculated for both 002 and 004 peaks shows a clear increase up to 35 years and then a slow rate decrease. This pattern after maturity is probably a characteristic of the ageing process and its detrimental effects and has been reported elsewhere by our group [41] when we tested trabecular bone from fracture and non-fracture neck of the femurs and found lower coherence length values in the fracture group. On the other hand, studies have shown that increased crystal size is associated with increased fragility [42,43] and that fragility is related to the heterogeneity of mineral crystal size [32,44]. Meanwhile crystal lattice parameters are linked to ion exchange which happen in order to fill vacancies caused by changes in crystal strain. Therefore, all the changes like the increase in crystal size with a reduction in coherence lengths, increased carbonate and ion substitutions result in a reduction in the overall health of the bone mineral (increase in disorder and non-stoichiometry), and this accompanies the deteriorating mechanical material properties at the bone tissue level.

4.3 Mechanical properties, water, and organic changes

With organic and mineral, water represents the essential third component of bone. It is present in various forms some of which is structurally associated with the organic and matrix moieties. Superficial water, non-associated with any other structure keep the collagen moist and has been shown to have an antagonistic effect between stiffness and toughness. Bound water is responsible for the electrostatic interaction of collagen molecules and provides stability and strength to the collagen fibrils [17]. The reduction in bound water is believed to reduce strength and increase stiffness [5,18] and this interplay was seen here with an increase in hardness and stiffness and an age-related reduction in structural water. It is not surprising that the majority of these changes are concentrated before maturity. Bones have to be elastic and tough in the young (giving rise to the so called 'green stick fractures') and progressively become stiffer but less tough towards maturity as the kind of demands placed on the skeleton in ontogeny change.

Decrease in organic content itself (apart from its hydration level) is expected to lead to a decrease in viscoelasticity and an increase in indentation creep. The state of the organic matrix was assessed in two main aspects: collagen integrity (thermal stability and level of hydration) and its amount (organic content). Thermal stability decreases consistently and linearly with age, and it has been shown to correlate with bone fragility through reduced bone toughness [8,45]. Elsewhere it has been shown that there is a clear reduction in collagen thermal stability in osteoporotic bone compared to the heathy control, and that even in healthy individuals it decreases linearly with age [8,46]. The present findings show a decrease in the capacity of cortical bone to absorb energy elastically and an increase in indentation creep both linked to a decrease in collagen thermal stability. As shown by experiments where the collagen component alone was compromised [47,48] this reduced toughness but did not alter stiffness. Investigations involving nanoindentation and spectroscopic analysis also provided evidence that collagen has an impact on the viscoelastic behaviour of bone matrix [11]. When considering the amount of organic matrix rather than its quality, we noticed that it negatively affects all indentation properties except for indentation creep. Bala et al. [11] claimed that collagen content related negatively to microhardness and positively to viscoelastic behaviour and here we saw a clear relationship to creep (viscoplasticity) and elastic work ratio. Reduction in amount of organic content is also expected to induce a decrease in the viscoelastic properties and an increase in indentation creep.

4.4 The collagen to mineral association

Recent work in the literature has focused on the investigations of nanoscale deformation mechanism of mineral and collagen by means of wide angle and small angle scattering X-ray diffraction in a synchrotron source [49-51]. The phenomena observed there may be very useful in providing insight for the yet unexplained issue of load transfer between mineral crystals and collagen fibres via the interfibrillar matrix. The integrity of this process seems to be compromised primarily by posttranslational modification of the collagenous matrix, the loss of bonds in the interfibrillar matrix, the accumulation of mature cross-links and advanced glycation end-products [52,53] with time in the body (tissue age) and with age (chronological age of the individual). Further studies are needed to investigate the relationship between tissue material properties and macroscale mechanical behaviour in the light of physicochemical changes of bone matrix and composition we saw here and for the nano level strain behaviour with respect to all such structural and functional aspects of bone.

4.5 Time sequence of events

The indentation modulus and hardness values increase to maturity <35 years and then decline in the remodelling phase. As shown in **Figure 6** this is due mostly on composition with increase in mineral (and by implication decrease in water and organic content) increasing stiffness and hardness. The indentation creep and the elastic work ratio behave complementary to each other, so the stiffer and more mineralised the material is the less energy it will dissipate plastically and the less it will creep. The second feature that C_{IT} and η_{IT} have in common is that they show the same decline and increase respectively throughout life with two slopes (**Fig. 3 D, E**) and without an inflection (up/down effect). The physicochemical parameter which behaves the same are those in **Fig. 5 A, C** pertaining to crystal chemistry and porosity. It is interesting that stiffness and hardness are directly and simply composition dependent while the energy/plasticity parameters C_{IT} and η_{IT} derive from a more intricate causal process involving composition, architecture, and porosity. Physicochemical changes of mineral and organic have been shown to play a central role in balancing mechanical behaviour. Crystallite length has been seen to increase, when it is allowed to mature in situ, but later responding to the balance in bone resorption/deposition it exists in a mixture of forms (mature and immature) reflecting the bone turnover process. In this study coherence length along $\langle 00\ell \rangle$ crystallographic direction increases in the first three decades (in situ maturation as tissue ages). According to composite material science crystallite length and its content are expected to increase stiffness but they also reduce toughness as the tissue capacity to yield reduces. When bone is overloaded, it will go into yield (elasto-plastic deformation) and if loaded further it will go through a ductile to brittle transition (DBT) which results into fracture. It has been seen recently that this DBT is age and load rate

related [12] with fast impact-like loading events in older individuals being stochastically more 'dangerous' than the same events for young individuals. The macroscopic properties examined in [12] happen at a higher length scale level and one may argue that the homogenised material features we examined here may be responsible for and able to underpin the mechanical integrity of bone at the macroscopic level. However, bone being such a complex system does not allow one to draw unequivocal conclusion on the present study alone.

4.6 Limitations

The present study has its limitations in the fact that it is cross-sectional following the evolution of bone tissue properties across a population as opposed along the life of single individuals. This makes sense in the physical and forensic anthropology field where we often require establishing as many ageing-trends as possible with the great variety of microanalytical methods we have at our disposal. In this sense if we were to sample randomly across a population, we would be able to expect the various parameters to fall within the boundaries of behaviour shown here in the various figures. In that case the expressions we use here on bone behaviour, under this caveat, is in fact the behaviour a clinician or a practising anthropologist will encounter when randomly selecting an individual from a similar cohort. The present cohort was that of a single ethnic Caucasian background, and in that sense, we do not know how the bone tissue will behave for other ethnicities or races.

A further limitation could be the use of ribs with the implication being that other skeletal sites may reveal other trends. However, we have presented similar trends for the clavicle of these same individuals [54] recently and the effects of using different bone from the thorax are barely noticeable. We now plan to combine the two datasets so that by using two bones from the same donor we hope to reduce the noise and variability between subjects, a potential bonus for forensic anthropology applications. The use of chloroform/methanol to remove the fat and marrow at preparation may have inadvertently dried the bone or remove some loose non collagenous (NCP) proteins. The present study is a laboratory physicochemical study where the priority is to engage in methods and protocols that favour the method first and then the material. Nanoindentation requires carefully degreasing of the samples and then it produces (in our experience) more reliable results when this removal of fat and marrow is performed first, before reconstituting the samples in PBS, drying them out and place them in resin for the mirror finish polishing procedure. With upper most in our mind to engage in preparation protocols that optimise the performance of our physicochemical methods we believe that it is easier to ascertain and maintain bone in its dry state than partially or variably hydrated tested and therefore, the nanoindentations were performed on dry specimens. We have applied this method for years and in every study of nanoindentation we have engaged in. Since our study is a cross populational study the likely effects on nanoindentation values will most likely be a shift in absolute values or nanoindentation modulus (accuracy) without affecting the trend across the wide age spectrum.

At the same time we cannot be explicit on the likely effect that this preparation protocol may have on the collagen of the mineral phase of bone, this has not been explored. Some of the loosely or structurally bound water may have been removed, but we have no evidence for this. We have been using simply warm water jet and/or chloroform/methanol to achieve degreasing and after drying/ashing we have noticed no discernible or statistically significant changes in the % values of the 3 main phases of bone as expressed here. This article explored the state and effect of the three main phases of bone namely mineral, collagen and water which are significant contributors to the mechanical behaviour of the material. In mechanistic terms these are: collagen the main structural protein of bone, HAp its reinforcing phase and water the medium which provides the environment in which bone exists. We did not explore or examined the so-called NCPs (non-collagenous proteins) which are part of the organic milieu and by all accounts they modulate and moderate [55,56] the presence and effect of the three main structural ingredients. NCP have been seen to alter in various musculoskeletal conditions and in disease and relate to the demonstrated properties of bone. However, one may argue that NCP are simply a part of a whole range of physical, chemical, and cellular mechanisms, which together with past history (fatigue damage accumulation), underpin the present state of bone as it manifests itself at any particular time. The present study looked in the manifested state of bone without explicitly exploring the underpinning contributors that make bone what it is.

5 Conclusions

We have looked in the bone micromechanical, composition and physicochemical properties in a cross-sectional study of a population of Caucasian origin and found that there is an age point at which most parameters exhibit a change in their age trends. The point at which skeletal maturity is reached in this cortical rib bone was seen by all accounts to be around 35years of age. The synchronous changes in structure, composition, properties and physicochemistry allude to a complex behaviour with interaction at all levels of bone's hierarchical structure which may have implications for both clinical and forensic bone analysis applications. However, these same results point to a broader need to expand this kind of knowledge to age-related changes for other skeletal elements as well as distinguish between cortical and trabecular bone as they have different turnover rates.

Contributors

Study Design: AB, PZ and EFK.; Study conduct: AB, PZ; Sample Collection: BX; Data Collection: AB; Data Analysis: AB, EA, PZ and EFK; Data Interpretation: AB, EA, PZ and EFK; Drafting Manuscript: AB, PZ, EFK; Supervision: PZ, EFK; Project administration: PZ; Resources: EFK, PZ; Approving final Manuscript: AB, PZ, BX, EFK; Responsibility for data integrity: AB.

Conflict of interest

The authors declare that they have no conflict of interest.

Funding

Andrea Bonicelli was in receipt of a fellowship by the University of Edinburgh to support his PhD studies. The testing and resources were provided via internal funding in both UK based institutions. The Forensic Institute in Tirana offered samples as 'in kind' contribution.

Ethics

The study protocol was approved by the Ethics Committee of the University of Edinburgh (Ethics Assessment Level 2) and the Institute of Forensic Medicine (Protocol Number 795/3 A. Xh.) in Tirana, Albania, and the material was further cleared by the NHS Lothian Tissue Governance (Protocol Number ICA01/17). Experimental procedures were carried under the Cranfield University Ethics Committee approval (CURES/2294/2017).

Research data sharing and availability

Data underlying this paper can be accessed at CORD (Cranfield Online Research Data) https://cranfield.figshare.com

Acknowledgements

The authors are grateful to Mr. Kostaq Beluri, of the Control Department Investigation and Prosecution of the General Prosecutor, Ministry of Head Justice, Tirana, Albania for granting permission to carry out the project and Emily Arnold with Keith D. Rogers for their invaluable help in XRD analysis.

References

[1] M.J. Olszta, X. Cheng, S.S. Jee, R. Kumar, Y.Y. Kim, M.J. Kaufman, E.P. Douglas, L.B. Gower, Bone structure and formation: A new perspective, Materials Science and Engineering R: Reports. 58 (2007) 77–116. https://doi.org/10.1016/j.mser.2007.05.001.

[2] J.Y. Rho, L. Kuhn-Spearing, P. Zioupos, Mechanical properties and the hierarchical structure of bone, Medical Engineering and Physics. 20 (1998) 92–102. https://doi.org/10.1016/S1350-4533(98)00007-1.

[3] A.L. Boskey, R. Coleman, Aging and Bone, Journal of Dental Research. 89 (2010) 1333–1348. https://doi.org/10.1177/0022034510377791.

[4] D.B. Burr, Changes in bone matrix properties with aging, Bone. 120 (2019) 85–93. https://doi.org/10.1016/j.bone.2018.10.010.

[5] M. Unal, S. Uppuganti, S. Timur, A. Mahadevan-Jansen, O. Akkus, J.S. Nyman, Assessing matrix quality by Raman spectroscopy helps predict fracture toughness of human cortical bone, Scientific Reports. 9 (2019) 7159. https://doi.org/10.1038/s41598-019-43542-7.

[6] Y. Bala, D. Farlay, P.D. Delmas, P.J. Meunier, G. Boivin, Time sequence of secondary mineralization and microhardness in cortical and cancellous bone from ewes, Bone. 46 (2010) 1204–1212. https://doi.org/10.1016/j.bone.2009.11.032.

[7] C. Combes, S. Cazalbou, C. Rey, Apatite biominerals, Minerals. 6 (2016) 1–26. https://doi.org/10.3390/min6020034.

[8] P Zioupos, J.D. Currey & A.J. Hamer, The role of collagen in the declining mechanical properties of aging human cortical bone., Journal of Biomedical Materials Research Part A, 45(2) (1999) 108-16.

[9] P. Zioupos, Ageing Human Bone: Factors Affecting its Biomechanical Properties and the Role of Collagen, Journal of Biomaterials Applications. 15 (2001). https://doi.org/10.1106/5JUJ-TFJ3-JVVA-3RJ0.

[10] X. Wang, X. Li, R.A. Bank, C.M. Agrawal, Effects of Collagen Unwinding and Cleavage on the Mechanical Integrity of the Collagen Network in Bone, Calcifed Tissue International. 71 (2002) 186–192. https://doi.org/10.1007/s00223-001-1082-2.

[11] Y. Bala, B. Depalle, T. Douillard, S. Meille, P. Clément, H. Follet, J. Chevalier, G. Boivin, Respective roles of organic and mineral components of human cortical bone matrix in micromechanical behavior: An instrumented indentation study, Journal of the Mechanical Behavior of Biomedical Materials. 4 (2011) 1473–1482. https://doi.org/10.1016/j.jmbbm.2011.05.017.

[12] P. Zioupos, H.O.K. Kirchner, H. Peterlik, Ageing bone fractures: The case of a ductile to brittle transition that shifts with age, Bone. 131 (2020) 115176. https://doi.org/10.1016/j.bone.2019.115176.

[13] I. Kontopoulos, S. Presslee, K. Penkman, M.J. Collins, Preparation of bone powder for FTIR-ATR analysis: The particle size effect, Vibrational Spectroscopy. 99 (2018) 167–177. https://doi.org/10.1016/j.vibspec.2018.09.004.

[14] A. Bonicelli, B. Xhemali, E.F. Kranioti, P. Zioupos, Rib biomechanical properties exhibit diagnostic potential for accurate ageing in forensic investigations, PLoS ONE. 12 (2017) 1–20. https://doi.org/10.1371/journal.pone.0176785.

[15] A. Bonicelli, P. Zioupos, E. Arnold, K.D. Rogers, B. Xhemali, E.F. Kranioti, Age related changes of rib cortical bone matrix and the application to forensic age - at - death estimation, Scientific Reports. 11 (2021) 1–13. https://doi.org/10.1038/s41598-021-81342-0.

[16] J-Y Rho, P. Zioupos, J.D. Currey, G.M. Phar, Variations in the individual thick lamellar properties within osteons by nanoindentation, Bone. 25 (1999) 295-300. doi: 10.1016/s8756-3282(99)00163-5.

[17] J. Kopp, M. Bonnet, J.P. Renou, Effect of Collagen Crosslinking on Collagen-Water Interactions (A DSC Investigation), Matrix. 9 (1989) 443–450. https://doi.org/10.1016/S0934-8832(11)80013-2.

[18] M. Unal, O. Akkus, Raman spectral classification of mineral- and collagen-bound water's associations to elastic and post-yield mechanical properties of cortical bone, Bone. 81 (2015) 315–326. https://doi.org/10.1016/j.bone.2015.07.024.

[19] E.P. Paschalis, S. Gamsjaeger, K. Klaushofer, Vibrational spectroscopic techniques to assess bone quality, Osteoporosis International. 28 (2017) 2275–2291. https://doi.org/10.1007/s00198-017-4019-y.

[20] T.J.U. Thompson, M. Islam, K. Piduru, A. Marcel, An investigation into the internal and external variables acting on crystallinity index using Fourier Transform Infrared Spectroscopy on unaltered and burned bone, Palaeogeography, Palaeoclimatology, Palaeoecology. 299 (2011) 168–174. https://doi.org/10.1016/j.palaeo.2010.10.044.

[21] G.K. Williamson, W.H. Hall, X-ray line broadening from filed aluminium and wolfram, Acta Metallurgica. 1 (1953) 22–31. https://doi.org/doi.org/10.1016/0001-6160(53)90006-6.

[22] S. Gosling, R. Scott, C. Greenwood, P. Bouzy, J. Nallala, I.D. Lyburn, N. Stone, K. Rogers, Calcification Microstructure Reflects Breast Tissue Microenvironment, Journal of Mammary Gland Biology and Neoplasia. 24 (2019) 333–342. https://doi.org/10.1007/s10911-019-09441-3.

[23] J.D. Currey, 'Bones: structure and mechanics' Princeton University Press, New Jersey (2002).

[24] J.D. Currey, K. Brear, P. Zioupos, Notch sensitivity of mammalian mineralized tissues in impact, Proceedings of the Royal Society of London. Series B: Biological Sciences. 271 (2004). https://doi.org/10.1098/rspb.2003.2634.

[25] J.S. Walsh, Normal bone physiology, remodelling and its hormonal regulation, Surgery. 33 (2015) 1–6. https://doi.org/10.1016/j.mpsur.2014.10.010.

[26] B. Clarke, Normal bone anatomy and physiology, Clinical Journal of the American Society of Nephrology : CJASN. 3 Suppl 3 (2008) 131–139. https://doi.org/10.2215/CJN.04151206.

[27] M.R. Bruce, D.B. Burr, Structure, Function, and Adaptation of Compact Bone, (1989) Raven Press, ISBN 13: 9780881675009.

[28] J.Y. Rho, P. Zioupos, J.D. Currey, G.M. Pharr, Microstructural elasticity and regional heterogeneity in human femoral bone of various ages examined by nano-indentation, Journal of Biomechanics. 35 (2002) 189–198. https://doi.org/10.1016/S0021-9290(01)00199-3.

[29] A. Parfitt, Skeletal heterogeneity and the purposes of bone remodelling: implications for the understanding of osteoporosis, Third Edit, Elsevier Inc., 1996. https://doi.org/10.1016/B978-0-12-370544-0.50007-0.

[30] C.E. Hoffler, K.E. Moore, K. Kozloff, P.K. Zysset, M.B. Brown, S.A. Goldstein, Heterogeneity of bone lamellar-level elastic moduli, Bone. 26 (2000) 603–609. https://doi.org/10.1016/S8756-3282(00)00268-4.

[31] K. Tai, M. Dao, S. Suresh, A. Palazoglu, C. Ortiz, Nanoscale heterogeneity promotes energy dissipation in bone, Nature Materials. 6 (2007) 454–462. https://doi.org/10.1038/nmat1911.

[32] A. Boskey, Bone mineral crystal size, Osteoporosis International. 14 (2003) 16–21. https://doi.org/10.1007/s00198-003-1468-2.

[33] P. Chavassieux, E. Seeman, P.D. Delmas, Insights into material and structural basis of bone fragility from diseases associated with fractures: How determinants of the biomechanical properties of bone are compromised by disease, Endocrine Reviews. 28 (2007) 151–164. https://doi.org/10.1210/er.2006-0029.

[34] G. Boivin, Y. Bala, A. Doublier, D. Farlay, L.G. Ste-Marie, P.J. Meunier, P.D. Delmas, The role of mineralization and organic matrix in the microhardness of bone tissue from controls and osteoporotic patients, Bone. 43 (2008) 532–538. https://doi.org/10.1016/j.bone.2008.05.024.

[35] Y. Bala, D. Farlay, G. Boivin, Bone mineralization : from tissue to crystal in normal and pathological contexts, Osteoporosis International. (2012). https://doi.org/10.1007/s00198-012-2228-y.

[36] E. Lefèvre, D. Farlay, Y. Bala, F. Subtil, U. Wolfram, S. Rizzo, C. Baron, P. Zysset, M. Pithioux, H. Follet, Compositional and mechanical properties of growing cortical bone tissue: a study of the human fibula, Scientific Reports. 9 (2019) 1–16. https://doi.org/10.1038/s41598-019-54016-1.

[37] L.J. Smith, J.P. Schirer, N.L. Fazzalari, The role of mineral content in determining the micromechanical properties of discrete trabecular bone remodeling packets, Journal of Biomechanics. 43 (2010) 3144–3149. https://doi.org/10.1016/j.jbiomech.2010.07.038.

[38] O. Akkus, F. Adar, M.B. Schaffler, Age-related changes in physicochemical properties of mineral crystals are related to impaired mechanical function of cortical bone, Bone. 34 (2004) 443–453. https://doi.org/10.1016/j.bone.2003.11.003.

[39] X. Bi, C.A. Patil, C.C. Lynch, G.M. Pharr, A. Mahadevan-Jansen, J.S. Nyman, Raman and mechanical properties correlate at whole bone- and tissue-levels in a genetic mouse model, Journal of Biomechanics. 44 (2011) 297–303. https://doi.org/10.1016/j.jbiomech.2010.10.009.

[40] R.G. Handschin, W.B. Stern, X-ray diffraction studies on the lattice perfection of human bone apatite (Crista Iliaca), Bone. 16 (1995). https://doi.org/10.1016/S8756-3282(95)80385-8.

[41] C. Greenwood, J. Clement, A. Dicken, J.P.O. Evans, I. Lyburn, R.M. Martin, K. Rogers, N. Stone, P. Zioupos, Towards new material biomarkers for fracture risk, Bone. 93 (2016) 55–63. https://doi.org/10.1016/j.bone.2016.09.006.

[42] A.S. Turner, J.M. Maillet, C. Mallinckrodt, L. Cordain, Bone mineral density of the skull in premenopausal women, Calcified Tissue International. 61 (1997) 110–113. https://doi.org/10.1007/s002239900305.

[43] J.S. Yerramshetty, O. Akkus, The associations between mineral crystallinity and the mechanical properties of human cortical bone, Bone. 42 (2008) 476–482. https://doi.org/10.1016/j.bone.2007.12.001.

[44] H. Fonseca, D. Moreira-Gonçalves, H.J.A. Coriolano, J.A. Duarte, Bone quality: The determinants of bone strength and fragility, Sports Medicine. 44 (2014) 37–53. https://doi.org/10.1007/s40279-013-0100-7.

[45] C.C. Danielsen, Age-related thermal stability and susceptibility to proteolysis of rat bone collagen, The Biochemical Journal. 272 (1990) 697–701.

[46] J.D. Currey, Role of collagen and other organics in the mechanical properties of bone, Osteoporosis International. 14 (2003) 29–36. https://doi.org/10.1007/s00198-003-1470-8.

[47] J.D. Currey, J. Foreman, I. Laketić, J. Mitchell, D.E. Pegg, G.C. Reilly, Effects of ionizing radiation on the mechanical properties of human bone, J Orthop Res. (1997)15(1):111-7. doi: 10.1002/jor.1100150116.

[48] H.S. Gupta, W. Wagermaier, G.A. Zickler, R.-B.D. Aroush, S.S. Funari, P. Roschger, H.D. Wagner, P. Fratzl, Nanoscale Deformation Mechanisms in Bone, Nano Letters. 5 (2005) 2108–2111. https://doi.org/10.1021/nl051584b.

[49] H.S. Gupta, S. Krauss, M. Kerschnitzki, A. Karunaratne, J.W.C. Dunlop, A.H. Barber, P. Boesecke, S.S. Funari, P. Fratzl, Intrafibrillar plasticity through mineral/collagen sliding is the dominant mechanism for the extreme toughness of antler bone, Journal of the Mechanical Behavior of Biomedical Materials. 28 (2013) 366–382. https://doi.org/10.1016/j.jmbbm.2013.03.020.

[50] E.A. Zimmermann, B. Busse, R.O. Ritchie, The fracture mechanics of human bone: influence of disease and treatment, BoneKEy Reports. 4 (2015) 1–13. https://doi.org/10.1038/bonekey.2015.112.

[51] S. Ma, E.L. Goh, T. Tay, C.C. Wiles, O. Boughton, J.H. Churchwell, Y. Wu, A. Karunaratne, R. Bhattacharya, N. Terrill, J.P. Cobb, U. Hansen, R.L. Abel, Nanoscale mechanisms in age-related hip-fractures, Scientific Reports. 10 (2020) 1–14. https://doi.org/10.1038/s41598-020-69783-5.

[52] A. Gautieri, F.S. Passini, U. Silván, M. Guizar-Sicairos, G. Carimati, P. Volpi, M. Moretti, H. Schoenhuber, A. Redaelli, M. Berli, J.G. Snedeker, Advanced glycation end-products: Mechanics of aged collagen from molecule to tissue, Matrix Biology. 59 (2017) 95–108. https://doi.org/10.1016/j.matbio.2016.09.001.

[53] M. Unal, S. Uppuganti, C.J. Leverant, A. Creecy, M. Granke, P. Voziyan, J.S. Nyman, Assessing glycation-mediated changes in human cortical bone with Raman spectroscopy, Journal of Biophotonics. 11 (2018) 1–15. https://doi.org/10.1002/jbio.201700352.

[54] H. McGivern, C. Greenwood, N. Marquez-grant, E.F. Kranioti, B. Xhemali, P. Zioupos, Age-related trends in the trabecular micro-architecture of the medial clavicle: Is it of use in forensic science? Frontiers in Bioengineering and Biotechnology. 7:467, (2019) doi.org/10.3389/fbioe.2019.00467.

[55] S. Morgan, A.A. Poundarik, D. Vashishth, Do Non-collagenous Proteins Affect Skeletal Mechanical Properties?, Calcified Tissue International. 97 (2015). https://doi.org/10.1007/s00223-015-0016-3.

[56] S. Bailey, G.E. Sroga, B. Hoac, O.L. Katsamenis, Z. Wang, N. Bouropoulos, M.D. McKee, E.S. Sørensen, P.J. Thurner, D. Vashishth, The role of extracellular matrix phosphorylation on energy dissipation in bone, ELife. 9 (2020). https://doi.org/10.7554/eLife.58184.

Figure captions

Figure 1. (A) Example of location for indentations in osteon and adjacent interstitial bone (O: osteon; I: interstitial bone); (B) The nanoindentation process (nomenclature as in CSM v3.75 users' manual) showing clockwise an indentation depth profile with depths before/during and after the load cycle; energy deposited plastically and recovered elastically by the material; a load/depth (F/h) curve and the creep (depth increase with time under load hold) parameter, all produced by the load-hold-unload indentation process.

Figure 2. Exploring non-linearity with a CR plot (component + residuals plot) in R 3.6.0. A component residual plot adds a line indicating where the line of best fit lies (solid purple line) with the regression on the raw data across all ages shown by the blue dashed line. There is a departure from linearity (slope of the purple curve) with a noticeable change in behaviour from 35 years onwards.

Figure 3. Five nanoindentation mechanical properties (each point the average of all indents produced for each donor) divided in two age ranges. They appear to follow a two-phase behaviour with at first an increase in indentation modulus and hardness and then after 35 years of age showing a decline (A-C). The behaviour of Creep (C_{IT}) and elastic work ratio (η_{IT}) parameters (D-E) showed the same trend throughout life (decreasing and increasing respectively with age), but again at 35 yrs the gradient changed noticeably. (Least squares regressions are shown with the 95% prediction interval for the data.)

Figure 4. Age related changes in matrix composition show a two-phase variation of (A) mineral, (B) water and (C) organic content. The drastic increase in mineral content before the age of 35 is coupled with the decrease in collagen and water content. After maturity there are no significant changes in composition other than a moderate decrease in mineral content. (Least squares regressions with the 95% prediction interval for the data.)

Figure 5. Certain parameters showed the same trend throughout life. (A) Porosity and (B) the carbonate to phosphate ratio of the bone mineral increased steadily from puberty to 85-90 years; (C) while the crystallinity index decreased. In all these three there was only a qualitative change of behaviour around this putative threshold age of maturity at 35, demonstrating itself by the scatter of the data. Quantitatively the slopes before and after 35 were the same. (Least squares regressions with the 95% prediction interval for the data.)

Figure 6. Relationship between mineral content and tissue mechanical properties shows how mineralisation appears to be an insightful causal factor for bone tissue properties. It can be seen that by being able to section the cohort in pre- and post-maturity we are able to distinguish clearly structure/function effects by using different symbols and so demonstrate that in the growing phase bone purposefully stiffens and hardens (blue circles), but once it acquires its peak it then maintains itself in a steady state with no cleat trends (yellow triangles). (Least squares regressions with the 95% prediction interval for the data.)

Fig 1

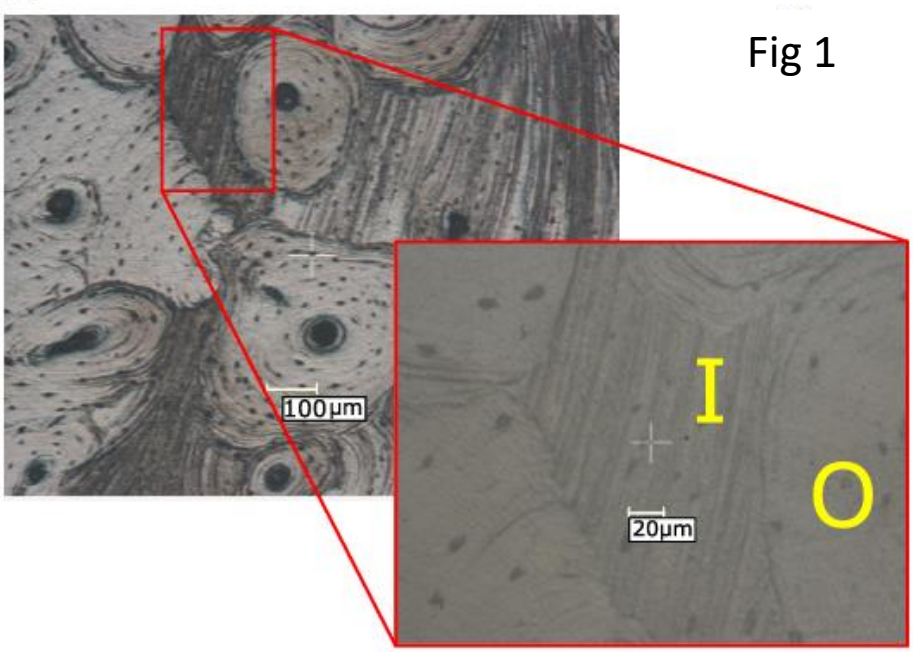
100 µm
I
O
20µm

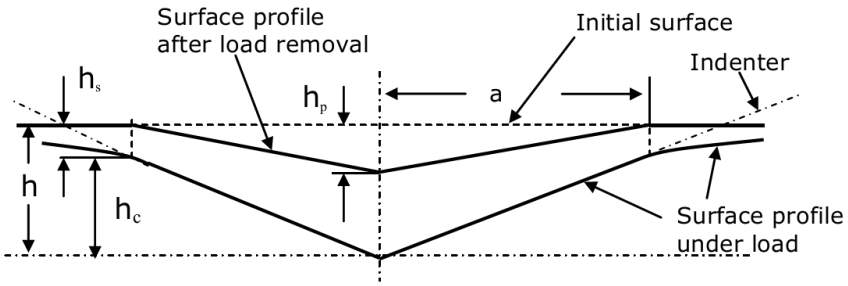
Surface profile
after load removal
Initial surface
Indenter
h_s
h_p
a
h
h_c
Surface profile
under load

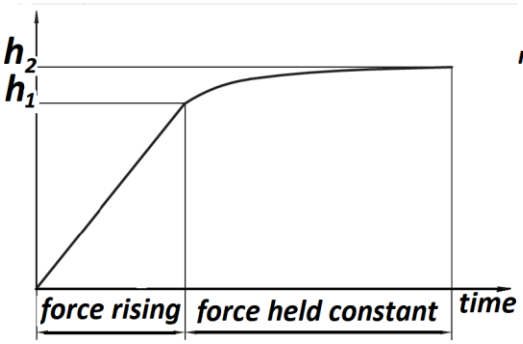
h_2
h_1
force rising
force held constant
time

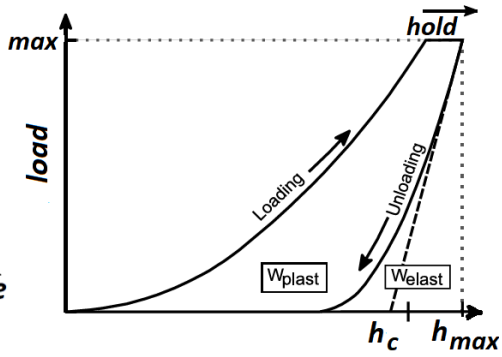
max
hold
load
Loading
Unloading
W_{plast}
W_{elast}
h_c
h_{max}

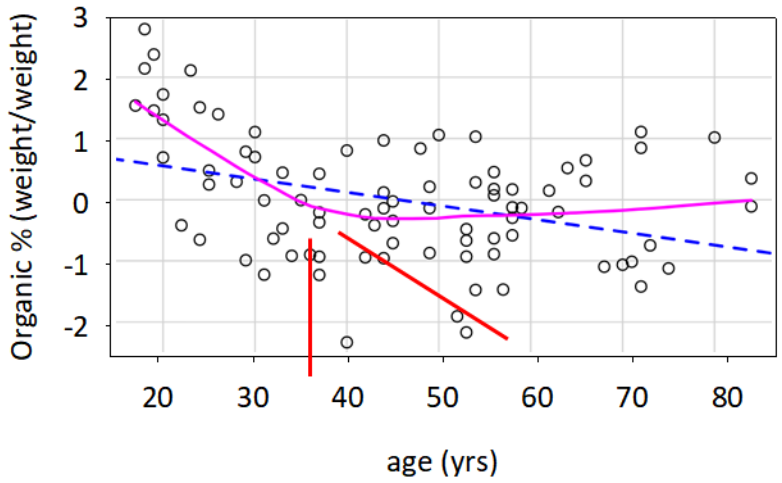

Fig. 2

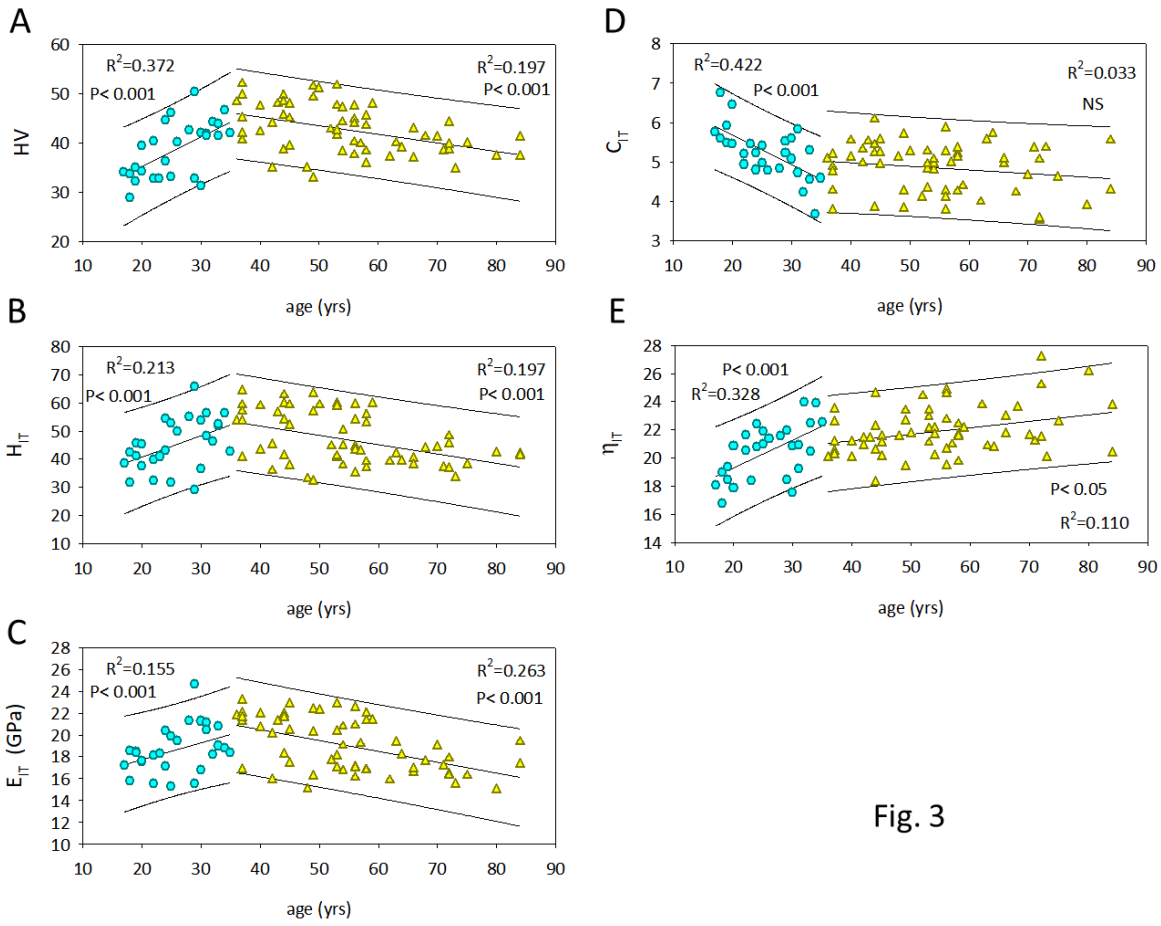
A
HV
R²=0.372
P< 0.001
R²=0.197
P< 0.001
age (yrs)
B
H_IT
R²=0.213
P< 0.001
R²=0.197
P< 0.001
age (yrs)
C
E_IT (GPa)
R²=0.155
P< 0.001
R²=0.263
P< 0.001
age (yrs)
D
C_IT
R²=0.422
P< 0.001
R²=0.033
NS
age (yrs)
E
η_IT
P< 0.001
R²=0.328
P< 0.05
R²=0.110
age (yrs)

Fig. 3

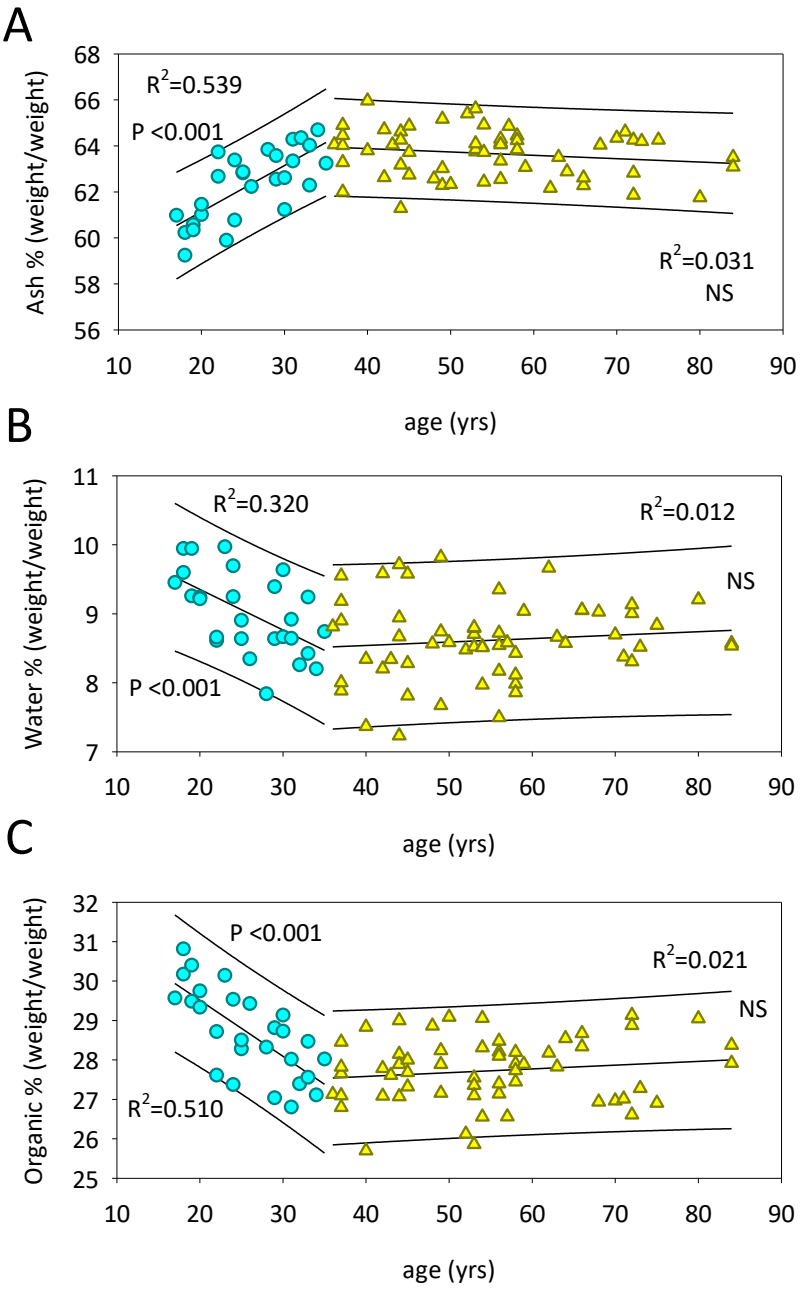
A
Ash % (weight/weight)
68
66
64
62
60
58
56
R2=0.539
P <0.001
R2=0.031
NS
10
20
30
40
50
60
70
80
90
age (yrs)
B
Water % (weight/weight)
11
10
9
8
7
R2=0.320
R2=0.012
NS
P <0.001
10
20
30
40
50
60
70
80
90
age (yrs)
C
Organic % (weight/weight)
32
31
30
29
28
27
26
25
P <0.001
R2=0.021
NS
R2=0.510
10
20
30
40
50
60
70
80
90
age (yrs)

Fig. 4

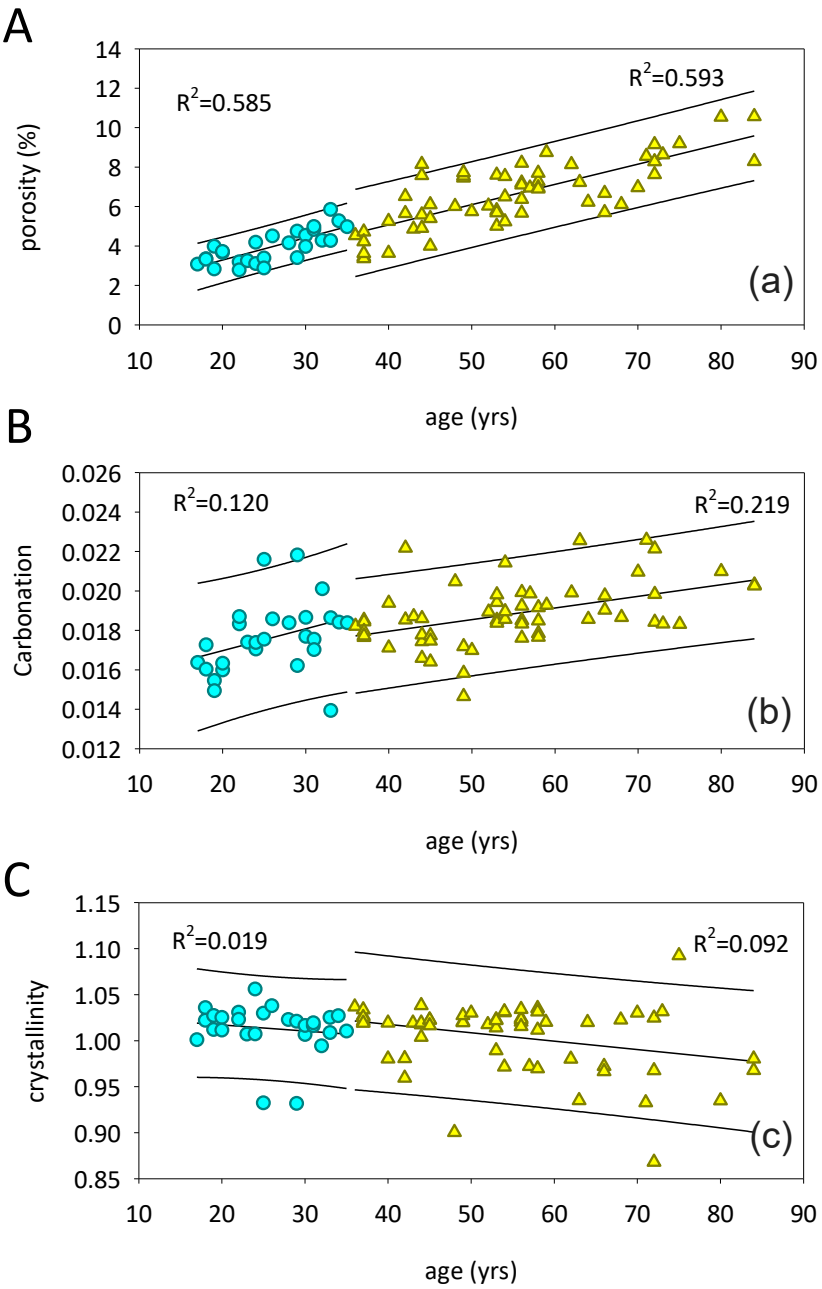
A
14
12
10
8
6
4
2
0
porosity (%)
R2=0.585
R2=0.593
(a)
10
20
30
40
50
60
70
80
90
age (yrs)
B
0.026
0.024
0.022
0.020
0.018
0.016
0.014
0.012
Carbonation
R2=0.120
R2=0.219
(b)
age (yrs)
C
1.15
1.10
1.05
1.00
0.95
0.90
0.85
crystallinity
R2=0.019
R2=0.092
(c)
age (yrs)

Fig. 5

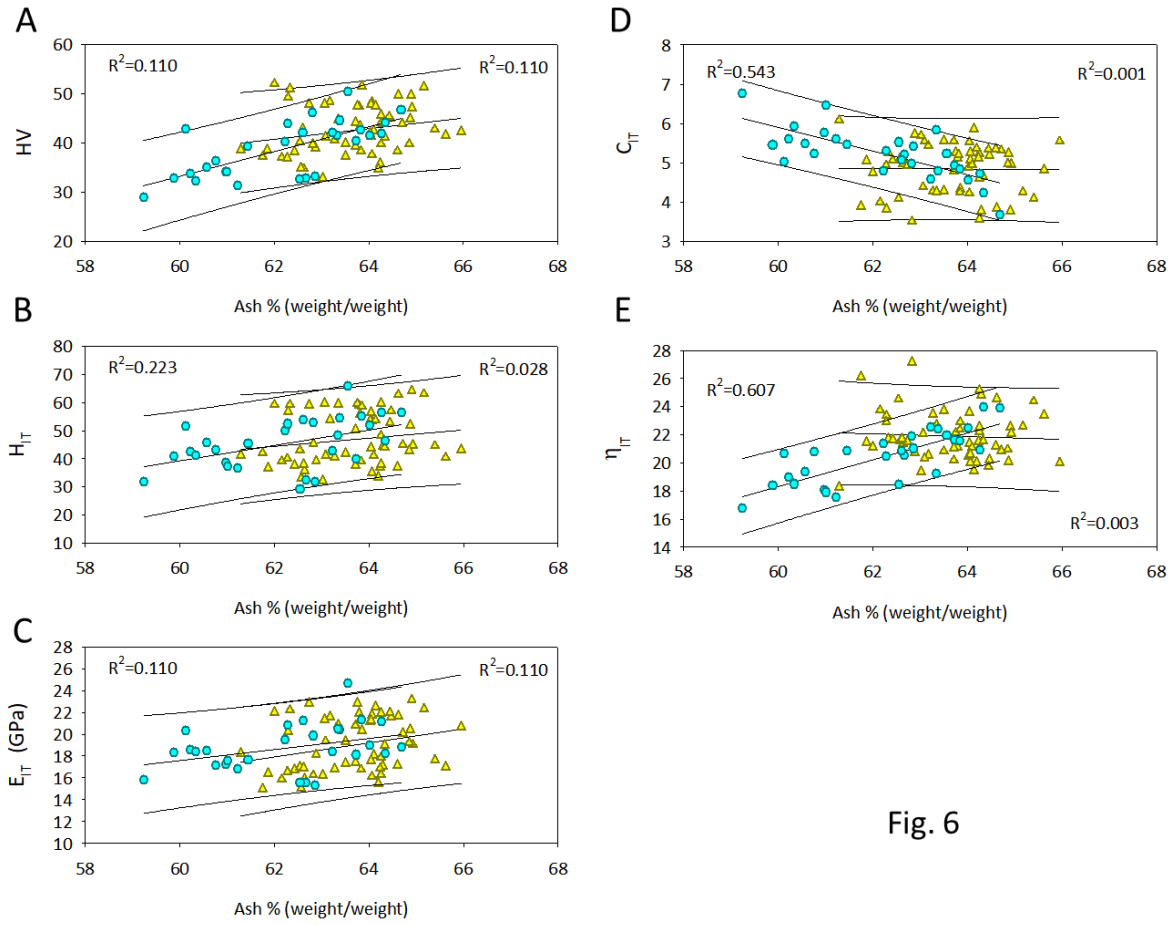
A
HV
R2=0.110
R2=0.110
Ash % (weight/weight)
B
HIT
R2=0.223
R2=0.028
Ash % (weight/weight)
C
EIT (GPa)
R2=0.110
R2=0.110
Ash % (weight/weight)
D
CIT
R2=0.543
R2=0.001
Ash % (weight/weight)
E
ηIT
R2=0.607
R2=0.003
Ash % (weight/weight)

Fig. 6